



1 **The importance of turbulent ocean-sea ice nutrient exchanges for** 2 **simulation of ice algal biomass and production with CICE6.1 and** 3 **Icepack 1.2**

4
5 Pedro Duarte¹, Philipp Assmy¹, Karley Campbell^{2,3}, Arild Sundfjord¹

6 ¹ Norwegian Polar Institute, Fram Centre, Tromsø, Norway

7 ² Department of Arctic and Marine Biology, UiT The Arctic University of Norway, Norway

8 ³ Bristol Glaciology Centre, University of Bristol, UK

9 *Correspondence to:* Pedro Duarte (Pedro.Duarte@npolar.no)

10 **Abstract.** Different sea-ice models apply unique approaches in the computation of nutrient diffusion between the ocean and
11 the ice bottom, which are generally decoupled from the calculation of turbulent momentum and heat flux. Often, a simple
12 molecular diffusion formulation is used. We argue that nutrient transfer from the ocean to sea ice should be as consistent as
13 possible with momentum and heat transfer, since all these fluxes respond to varying forcing in a similar fashion. We
14 hypothesize that biogeochemical models which do not consider such turbulent nutrient exchanges between the ocean and the
15 sea-ice underestimate bottom-ice algal production. The Los Alamos Sea Ice Model (CICE + Icepack) was used to test this
16 hypothesis by comparing simulations with molecular and turbulent diffusion of nutrients into the bottom of sea ice,
17 implemented in a way that is consistent with turbulent momentum and heat exchanges. Simulation results support the
18 hypothesis, showing a significant enhancement of ice algal production and biomass when nutrient limitation was relieved by
19 bottom-ice turbulent exchange. Our results emphasize the potentially critical role of turbulent exchanges to sea ice algal
20 blooms, and the importance of thus properly representing them in biogeochemical models. The relevance of this becomes even
21 more apparent considering ongoing trends in the Arctic Ocean, with a predictable shift from light to nutrient limited growth of
22 ice algae earlier in the spring, as the sea ice becomes more fractured and thinner with a larger fraction of young ice with thin
23 snow cover.

24 **1 Introduction**

25 Momentum, heat and mass fluxes between the ocean and the sea-ice are of utmost importance to predict sea-ice motion,
26 thermodynamics, and biogeochemistry. Considering the interlinks between these processes one would expect that sea-ice
27 models used a common approach to compute them, notwithstanding their obvious specificities. However, when we look at
28 models published over the last decades, we find not only inter-model differences in the physical concepts used to describe the
29 processes responsible for some of the above fluxes, but also intra-model differences in the approaches used in calculating, for
30 example, heat and mass fluxes. In this work we will focus on the differences related with the vertical diffusion of tracers



31 between the water column and the bottom-ice and attempt to explore their consequences on nutrient limitation for sea-ice algal
32 growth.

33 The most common processes found in the literature to model nutrient exchanges between the water and the sea ice are based
34 on entrapment during freezing, release during melting and diffusive or convective fluxes (e.g. Arrigo et al., 1993; Jin et al.,
35 2006; Tedesco and Vichi, 2010; Jeffery et al., 2011). Arrigo et al. (1993) distinguished nutrient exchanges resulting from
36 gravity drainage in brine channels, from brine convection in the skeletal layer, dependent on the ice growth rate. These brine
37 fluxes were used to calculate nutrient exchanges as a diffusive process. Lavoie et al. (2005) also calculated nutrient exchanges
38 as a diffusive process. Jin et al. (2006; 2008) computed nutrient fluxes across the bottom layer as an advection process
39 dependent on ice growth rate and based on Wakatsuchi and Ono (1983). Molecular diffusion was also considered. More
40 recently, other authors have integrated formulations based on hydrostatic instability of brine density profiles, to compute brine
41 gravity drainage and tracer exchange between the ice and sea water, based on diffusive (Vancoppenolle et al., 2010; Jeffery et
42 al., 2011) or convective processes (Turner et al., 2013).

43 Interestingly, the resulting calculation of momentum and heat exchange versus salinity in models is often mismatched. In the
44 case of the former two, typically, a transfer mechanism (turbulent or not) between the ocean and the sea ice is not dependent
45 on any type of brine exchange. In the case of salinity, such a mechanism is not considered (e.g. Vancoppenolle et al., 2007;
46 Turner et al., 2013). Presumably, such differences result from the relative importance of various physical processes for different
47 tracers. Momentum and heat transfer between the ice and the water are fundamental mechanisms in explaining sea-ice
48 dynamics and thermodynamics, irrespective of brine exchanges. However, ice desalination depends mostly on brine drainage
49 and flushing during melt.

50 Vertical convective mixing of nutrients under the sea ice may result from brine rejection and/or drainage from the sea ice (Lake
51 and Lewis, 1970; Niedrauer and Martin, 1979; Reeburgh, 1984) and from turbulence due to shear instabilities generated by
52 drag at the ice-ocean interface (Gosselin et al., 1985; Cota et al., 1987; Carmack, 1986), internal waves and topographical
53 features (Ingram et al., 1989; Dalman et al., 2019). Gosselin et al. (1985) and Cota et al. (1987) stressed the significance of
54 tidally induced mixing in supplying nutrients to sympagic algae. Biological demand for silicic acid (hereafter abbreviated as
55 silicate) and nitrate is limited by the physical supply (Cota and Horne, 1989; Cota and Sullivan, 1990). Vertical nutrient fluxes
56 between the water and the bottom ice can be calculated from:

$$57 \quad F_c = -K_z \frac{\Delta C}{\Delta z}, \quad (1)$$

58 where K_z is the vertical eddy diffusivity ($\text{m}^2 \text{d}^{-1}$) and ΔC is the difference in nutrient concentration over the vertical distance
59 Δz (mmol m^{-4}) (Cota et al., 1987).

60 Even though this eddy diffusion approach was proposed more than 30 years ago, it has been rarely used in the literature. Table
61 1 summarizes several models published over the last decades and their approaches to the calculation of nutrient diffusion
62 between the ocean and bottom-ice. Some models do not consider this process and limit nutrient exchanges to brine dynamics
63 and/or entrapment during freezing and release during melting. Only one of the sampled models (Mortenson et al., 2017) uses



64 a parameterization based on friction velocity, whereas the others either do not consider nutrient diffusion or use molecular
 65 diffusion.
 66 From this assessment one may divide the ocean-ice exchange processes of existing biogeochemical models into those related
 67 to: (i) entrapment during freezing; (ii) brine drainage, driven by density instability; (iii) flushing, driven by snow and ice
 68 melting, and (iv) diffusive exchanges at the interface between the ocean and the ice, dependent on concentration gradients. In
 69 the absence of ice growth and when brine drainage is limited, diffusive nutrient exchanges between the ocean and the ice have
 70 the capacity to limit primary production. This limitation will be alleviated in the presence of a turbulent exchange mechanism.
 71 We argue that nutrient transfer should be as consistent as possible with momentum and heat transfer since all these fluxes are
 72 closely linked. We hypothesize that models which do not consider turbulent nutrient exchanges between the ocean and the sea-
 73 ice may underestimate bottom-ice ice algal production. Such underestimation will bias the role of sea ice algae in ice associated
 74 food webs and ecosystem services, such carbon dioxide exchanges and their climate feedbacks.
 75 To test the above hypothesis, we use a 1D vertically resolved model and contrast results using the default molecular diffusion
 76 parameterization and a “turbulent” parameterization analogous to that of momentum and heat transfer, based on McPhee
 77 (2008).

78

79 **Table 1. Model parameterizations used/proposed by different authors to compute diffusion of nutrients at the ice-ocean interface,**
 80 **independent of brine exchanges and/or ice growth/melting. The only example based on friction velocity is that of Mortenson et al.**
 81 **(2017). “None” is used when exchange processes depend solely on brine exchanges and/or ice growth/melting.**

Source	Type of diffusion	Associated model
Cota et al. (1987)	Eddy diffusion	-
Arrigo et al. (1993)	None	A simulated Antarctic fast ice ecosystem
Lavoie et al. (2005)	Molecular diffusion ($1 \times 10^{-9} \text{ m}^2 \text{ s}^{-1}$)	Ice algal modelling of the Arctic in Resolute Passage, Canadian archipelago.
Jin et al. (2006; 2008)	Molecular diffusion according to the authors but using a diffusion coefficient ($1.0 \times 10^{-5} \text{ m}^2 \text{ s}^{-1}$) that is 4 orders of magnitude higher than molecular diffusion of salt [$1.0 \times 10^{-9} \text{ m}^2 \text{ s}^{-1}$, following Mann and Lazier (2005)]	Ice-ocean ecosystem model for 1-D and 3-D applications in the Bering and Chukchi seas.
Tedesco and Vichi (2010 and e.g. 2019)	None	Biogeochemical flux model in sea ice
Vancoppenolle et al. (2010)	None	Modelling brine and nutrient dynamics in Antarctic sea ice
Mortenson et al. (2017)	Diffusion parameterized as a function of friction velocity	Biogeochemical model representing the low trophic levels of sea ice and pelagic ecosystems in the Arctic.
Hunke et al. (2016)	Molecular diffusion	Los Alamos Sea Ice Model



82 2 Methods

83 2.1 Concepts

84 Eq. (1) from Cota et al. (1987) provides the basis for our reasoning about nutrient exchanges between the ocean and the sea-
85 ice bottom being based on a turbulent exchange process, irrespective of other exchanges based on brine dynamics, ice melt
86 and ice growth. Turbulent exchanges may be parameterized through the flux of a quantity at the ocean-ice interface, calculated
87 as the product of a scale velocity and the change in the quantity from the boundary to some reference level (McPhee, 2008):

$$88 \langle w' S' \rangle = \alpha_s u^* (S_w - S_0) \quad (2)$$

89 Where, α_s is an interface salt/nutrient exchange coefficient (dimensionless); u^* is the friction velocity (m s^{-1}); S_0 and S_w are
90 sea-ice interface and far-field salinities, respectively.

91 Hereafter we will assume that salt turbulent exchanges are similar to nutrient exchanges and governed by the same principles
92 and parameters. The main difference between turbulent heat and salt/nutrient exchanges is due to the exchange coefficients
93 that may be higher for heat. The heat exchange coefficient (α_h) is around 0.006. The ratio (R) between α_h and α_s may vary from
94 unity to a range between 35 and 70 during ice melt and because of double diffusion (McPhee et al., 2008).

95 The net downward heat flux from the ice to the ocean in the Los Alamos Sea Ice Model (CICE + Icepack) is given by (Hunke
96 et al., 2015) and it is computed according to MCPhee et al. (2008) [Eq. (2)]:

$$97 F_{bot} = -\rho_w c_w \alpha_h u^* (T_w - T_f) \quad (3)$$

98 Where, ρ_w is the density of seawater (kg m^{-3}); c_w is the specific heat of seawater ($\text{J kg}^{-1} \text{K}^{-1}$); α_h is the heat transfer coefficient
99 (dimensionless); T_w is the water temperature (K); T_f if the freezing temperature (K).

$$100 [W m^{-2}] = [kg m^{-3}] [J kg^{-1} K^{-1}] [dimensionless] [m s^{-1}] [K]$$

101 We calculate salt or nutrient exchanges using a similar approach:

$$102 F_N = -\alpha_s u^* (N_w - N_i) \quad (4)$$

103 In fact, this agrees with MCPhee (2008) (see page 112, Fig. 6.3).

$$104 [g m^{-2} s^{-1}] = [dimensionless] [m s^{-1}] [g m^{-3}]$$

105 A timescale for this turbulent process may be calculated from:

$$106 \tau = \frac{\alpha_s u^*}{H} [s^{-1}] \quad (5)$$

107 Where H is the vertical distance over which diffusion is to be calculated (m). In the Los Alamos Sea Ice Model, it corresponds
108 to the layer thickness of the biogeochemical grid (biogrid) (Jeffery et al., 2017). The above time scale is calculated for
109 consistency with CICE implementation of diffusion, where a comparable time scale is calculated as:

$$110 \tau = \frac{Dm}{H^2} [s^{-1}] \quad (6)$$

111 Where Dm is the molecular diffusion coefficient. Eq. (5) or (6) must be multiplied by ice porosity and then used to compute
112 matrix coefficients for the Icepack transport equation along the biogrid (Hunke et al., 2016). Therefore, the implementation of



113 turbulent diffusion nutrient exchanges in terms consistent with momentum and heat exchanges is quite straightforward
114 depending on changing the timescales from Eq. (6) to (5).

115 **2.2 Implementation**

116 We used the Los Alamos Sea Ice Model, which is managed by the CICE Consortium with an active forum
117 (<https://bb.cgd.ucar.edu/cesm/forums/cice-consortium.146/>) and a git repository (<https://github.com/CICE-Consortium>). It
118 includes two independent packages: CICE and Icepack. The former computes ice dynamic processes and the latter ice column
119 physics and biogeochemistry. Their development is handled independently with respect to the GitHub repositories
120 (<https://github.com/CICE-Consortium>). All the changes described below were implemented in two forks to the above
121 repository, one for Icepack and another for CICE and they may be found in Duarte (2021a and b, respectively).

122 Our simulations may be run using only Icepack, since they are focused on ice column physics and biogeochemistry, without
123 the need to consider ice dynamic processes. However, we used both CICE + Icepack together to allow for use of netCDF based
124 input/output not included in Icepack. Therefore, we defined a 1D vertically resolved model with 1 snow layer and 15 ice layers
125 and 5X5 horizontal cells. This is the minimum number of cells allowable in CICE due to the need to include halo cells (only
126 the central “column” is simulated). Therefore, ice column physics and biogeochemistry were calculated by Icepack but CICE
127 was the model driver. The input file (`ice_in`) used in this study was included in our CICE fork and it lists all parameters used
128 in the model and described in Hunke et al. (2016), Jeffery et al. (2016), Duarte et al. (2017) and in Tables S1 and S2. Any
129 changes in “default” parameters or any other model settings will be specified.

130 We made several modifications in CICE to allow using forcing time series collected during the Norwegian Young Sea Ice
131 Expedition (N-ICE2015) (Granskog et al., 2018) and described in Duarte et al. (2017) (see Fig. 2 of the cited authors). These
132 modifications were meant to allow reading of forcing data at higher frequencies than possible with the standard input
133 subroutines in the CICE file `ice_forcing.F90`.

134 When the dynamical component of CICE is not used, u^* is set to a minimum value instead of being calculated as a function of
135 ice-ocean shear stress (Hunke et al., 2015). Duarte et al. (2017) implemented shear calculations from surface current velocities
136 (one of the models forcing functions) irrespective of using or not the CICE dynamics code. These modifications were also
137 incorporated in the current model configuration so that shear can be used to calculate friction velocity and, thereafter, influence
138 heat and tracer/nutrient exchanges, following Eqs. (3) and (4) and parameters described in McPhee et al. (2008). When the
139 parameter `kdyn` is set to zero in `ice_in`, ice dynamics is not computed, but shear is calculated in the modified subroutine
140 `icepack_step_therm1`, file `icepack_therm_vertical.F90`. If `kdyn` is not zero, these calculations are ignored since shear is already
141 calculated in the dynamical part of the CICE code.

142 A Boolean parameter (`Bottom_turb_mix`) was added to the input file, which is set to “false” or “true” when the standard
143 molecular diffusion approach or the new turbulent based diffusion approach is to be used, respectively. Another Boolean
144 (`Limiting_factors_file`) was added to the `ice_in` file. When set to “true” limiting factor values for light, temperature, nitrogen,



145 and silicate are written to a text file every model timestep. These are calculated by Icepack biogeochemistry, according to
146 Jeffery et al. (2016), but there is no writing-output option in the standard code.

147 **2.3 Model simulations**

148 Simulations were run for a refrozen lead (RL) without snow cover and for second-year sea ice (SYI) with ~40 cm snow cover
149 monitored in April-June during the N-ICE2015 expedition (Granskog et al., 2018 and Fig. 1 of Duarte et al. 2017). We ran
150 simulations with the standard formulations for biogeochemical processes described in Jeffery et al. (2016) and settings
151 described in Duarte et al. (2017), using mushy thermodynamics, vertically resolved biogeochemistry, and including: brine
152 drainage, freezing, flushing (Turner et al., 2013, Jeffery et al., 2016) and molecular diffusion as nutrient and algal biomass
153 exchange mechanisms between the ocean and sea ice. We contrasted the above simulations against others that replaced
154 molecular diffusion of nutrient exchange at the ice-ocean interface with turbulent diffusion (Table 2), calculated similar to heat
155 and momentum and following the parameterization described in McPhee et al. (2008) and detailed above. This contrast
156 provides insight into the effects of changing from molecular to turbulent nutrient diffusion on ice algal production (mg C m^{-2}
157 d^{-1}), chlorophyll standing stocks ($\text{mg Chl } a \text{ m}^{-2}$) and vertical distribution of chlorophyll concentration ($\text{mg Chl } a \text{ m}^{-3}$) [note
158 that CICE model output for algal biomass in mmol N m^{-3} was converted to $\text{mg Chl } a \text{ m}^{-3}$ as in Duarte et al. (2017), using 2.1
159 $\text{mg Chl } a \text{ mmol N}^{-1}$ and following Smith et al. (1993)]. However, due to the concurrent effects of algal biomass exchange
160 between the ocean and ice, such a contrast is not enough to explicitly test our hypothesis and conclude about the effects of
161 turbulent -driven nutrient supply on ice algal nutrient limitation. Therefore, simulations were also run contrasting molecular
162 and turbulent nutrient diffusion, as described above, but restarting from similar algal standing stocks and vertical distributions
163 within the ice and, switching off algal inputs from the water to the ice. This was done by nullifying the variable `algalN`, defining
164 the ocean surface background ice algal concentration, in file `icepack_zbgc.F90`, subroutine `icepack_init_ocean_bio` and in the
165 restart files. In the case of the RL simulations that started with zero ice, first a simulation was run until the 12 May, and then
166 the obtained ice conditions were used to restart new simulations without algal inputs from the ocean (`algalN = 0 mmol N m`
167 $^{-3}$). This way, when the simulations restarted, there was already an ice algal standing stock necessary for the modelling
168 experiments developed herein. The SYI simulations were, by default, “restart simulations”, beginning with observed ice
169 physical and biogeochemical variables. Therefore, there was already an algal standing stock in the ice from the onset (Text S1
170 and Table S3).

171 McPhee et al. (2008) estimated different values for α_s depending on whether the sea ice is growing (highest value) or melting
172 (lowest value) (Table 2). When running simulations with turbulent bottom diffusion for the RL, in some cases, we used only
173 the minimum or the maximum values for α_s to allow for a more extreme contrast between molecular and turbulent diffusion
174 parameterizations. This was done since the former value will tend to minimize differences, whereas the latter will tend to
175 emphasize them. We also completed simulations for the RL and for SYI changing between the maximum and the minimum
176 values of α_s , when ice was growing or melting, respectively, and following McPhee et al. (2008) (see Table 2 for details). This



177 parameterization with a variable α , is likely the most realistic one, accounting for double diffusion during ice melting (McPhee
178 et al., 2008).

179 Apart from contrasting the way bottom-ice exchanges of nutrients were calculated, some simulations contrasted different
180 parameters related to silicate limitation (Table 2). This approach follows Duarte et al. (2017), where simulations were tuned
181 by changing the Si:N ratio and the half saturation constant for silicate uptake because silicate limitation was leading to an
182 underestimation of algal growth. From this exercise we were able to assess if such tuning was still necessary after implementing
183 turbulent diffusion at the ice-ocean interface. Moreover, we repeated simulations with varying snow heights to further
184 investigate the interplay between light and nutrient limitation under molecular and turbulent nutrient diffusion (Table 2).

185 Details on model forcing with atmospheric and oceanographic data collected during the N-ICE2015 expedition, including
186 citations and links to the publicly available datasets are given in Fig. 2 and section 3 of Duarte et al. (2017) and in the
187 supplementary information. These data sets include: wind speed, air temperature, precipitation, and specific humidity (Hudson
188 et al., 2015); incident surface short and longwave radiation (Hudson et al., 2016); ice temperature and salinity (Gerland et al.,
189 2017); sea surface current velocity, temperature, salinity and heat fluxes from a turbulence instrument cluster (TIC) (Peterson
190 et al., 2016); sea surface nutrient concentrations (Assmy et al., 2016) and sea-ice biogeochemistry (Assmy et al., 2017). Model
191 forcing files may be found in Duarte (2021c).

192

193

194

195

196

197

198

199

200

201

202

203

204

205

206

207



208 **Table 2. Model simulations. Refrozen lead (RL) simulation RL_Sim1 corresponds to RL_Sim5 described in Duarte et al. (2017) - the**
 209 **simulation leading to a best fit to the observations in that study. The remaining RL simulations 2 – 5 differ from RL_Sim1 in using**
 210 **turbulent diffusion at the ice-ocean interface for nutrients in a comparable way as it is calculated for heat. Moreover, RL_Sim5**
 211 **differs in the concentration of ice algae in the water column that colonize the sea ice bottom (algalN) and in silicate limitation related**
 212 **parameters. These changes were done iteratively to fit the model to the observations. In RL_Sim2 and RL_Sim3 the maximum**
 213 **($\alpha_s=0.006$) and the minimum ($\alpha_s=0.006/70=8.6 \times 10^{-5}$) values recommended by McPhee et al. (2008), respectively, are used throughout**
 214 **the simulations, to provide extreme case scenarios for comparison with RL_Sim1. In RL_Sim4, $\alpha_s=8.6 \times 10^{-5}$ when ice is not growing**
 215 **and 0.006 otherwise, as recommended by McPhee et al. (2008), to account for double diffusive processes during ice melting that slow**
 216 **down mass exchanges. The remaining RL simulations (RL_Sim6-9) are like the previous ones (RL_Sim1-4, respectively), except for**
 217 **algalN that was set to zero mmol N m^{-3} , and all simulations were restarted with the same values for all variables. Therefore,**
 218 **simulations 6 – 9 may differ only from 13 May 2015, when they were restarted. Second year ice simulation SYI_Sim_1 is based on**
 219 **Duarte et al. (2017) SYI_Sim4 but without algal motion. SYI_Sim2 and SYI_Sim3 use turbulent diffusion at the ice-ocean interface.**
 220 **The former uses a decreased half saturation constant for silicate uptake, just like SYI_Sim1, whereas the latter uses the standard**
 221 **CICE value. The remaining SYI simulations (SYI_Sim4 and 5) are like SYI_Sim1 and 2, except for algalN that was set to zero.**
 222 **Simulations SYI_Sim1 and SYI_Sim2 were repeated but with different initial snow thickness of 30, 20 and 15 cm to further**
 223 **investigate the interplay between light and silicate limitation (see text).**

224

	Name	Description
Refrozen lead simulations	RL_Sim1	Standard CICE parameters, except for: (i) decreased Si:N ratio from 1.8 to 1.0, well within published ranges (e.g. Brzezinski, 1985; Hegseth, 1992); (ii) decreased half saturation constant for silicate uptake proportionately as the previous ratio, from 4.0 to 2.2 mM within published limits (e.g. Nelson and Treguer, 1992); (iii) decreased colonization in the same proportion as previous parameters by setting ice algal concentration in the water column (algalN) to $11 \times 10^{-4} \text{ mmol N m}^{-3}$.
	RL_Sim2	As RL_Sim1 but with molecular diffusivity at the ice-ocean interface replaced with turbulent exchanges, always using the highest value for α_s , as recommended by McPhee et al. (2008).
	RL_Sim3	As RL_Sim2 but always using the lowest value for α_s , as recommended by McPhee et al. (2008).
	RL_Sim4	As RL_Sim3 but using either the lowest value for α_s , as recommended by McPhee et al. (2008), when ice is not growing, or the highest one, otherwise.
	RL_Sim5	As RL_Sim4 but changing half saturation constant for silicate uptake to 5.0 mM and Si:N to 1.7. Moreover, algalN was reduced to $4 \times 10^{-4} \text{ mmol N m}^{-3}$.
	RL_Sims6-9	As RL_Sim1-4, respectively, except for algalN that was set to zero, and all simulations were restarted with the same values for all variables in the 13 May 2015.



Second year ice simulations	SYI_Sim1	Standard CICE parameters, except for: (i) the sigma coefficient for snow grain (R_{snw}) (Urrego-Blanco et al., 2016) that was reduced from 1.5 to 0.8 following Duarte et al. (2017) and (ii) the decreased Si:N ratio and the reduced half saturation constant for silicate uptake and algalN as in RL_Sim1 above
	SYI_Sim2	As SYI_Sim1 but with molecular diffusivity at the ice-ocean interface replaced with turbulent exchanges using either the lowest value for a_s , as recommended by McPhee et al. (2008), when ice is not growing, or the highest one, otherwise.
	SYI_Sim3	As SYI_Sim2 but changing half saturation constant for silicate uptake back to CICE original value (4.0 mM).
	SYI_Sim4 and 5	As SYI_Sim1 and 2, respectively, except for algalN that was set to zero.

225

226 3. Results

227 The results of the simulations listed in Table 2 and presented below may be found in Duarte (2021d).

228 3.1 Refrozen lead simulations

229 All simulations with turbulent diffusion (RL_Sim2 – RL_Sim5, Table 2), predict higher bottom chlorophyll *a* (*Chl a*)
 230 concentration than with the standard molecular diffusion formulation (RL_Sim1) (Fig. 1a). Simulations RL_Sim2 - 4 grossly
 231 overestimate observations. Simulation RL_Sim3, using the lowest value for α_s , is closer both to observations and to RL_Sim1,
 232 as well as RL_Sim5, with the latter having the same α_s values of RL_Sim4 but a half saturation constant for silicate limitation
 233 increased from its tuned value in Duarte et al. (2017) of 2.2 μM to 5.0 μM and algalN reduced (Table 2) to bring model results
 234 closer to observations. Patterns between simulations for the whole ice column and considering both standing stocks and net
 235 primary production, are similar to those observed for the bottom-ice (Fig. 1b). Algal biomass is concentrated at the bottom
 236 layers (Fig. 2). Concentrations in the layers located between the bottom and the top of the brine network (green lines in the



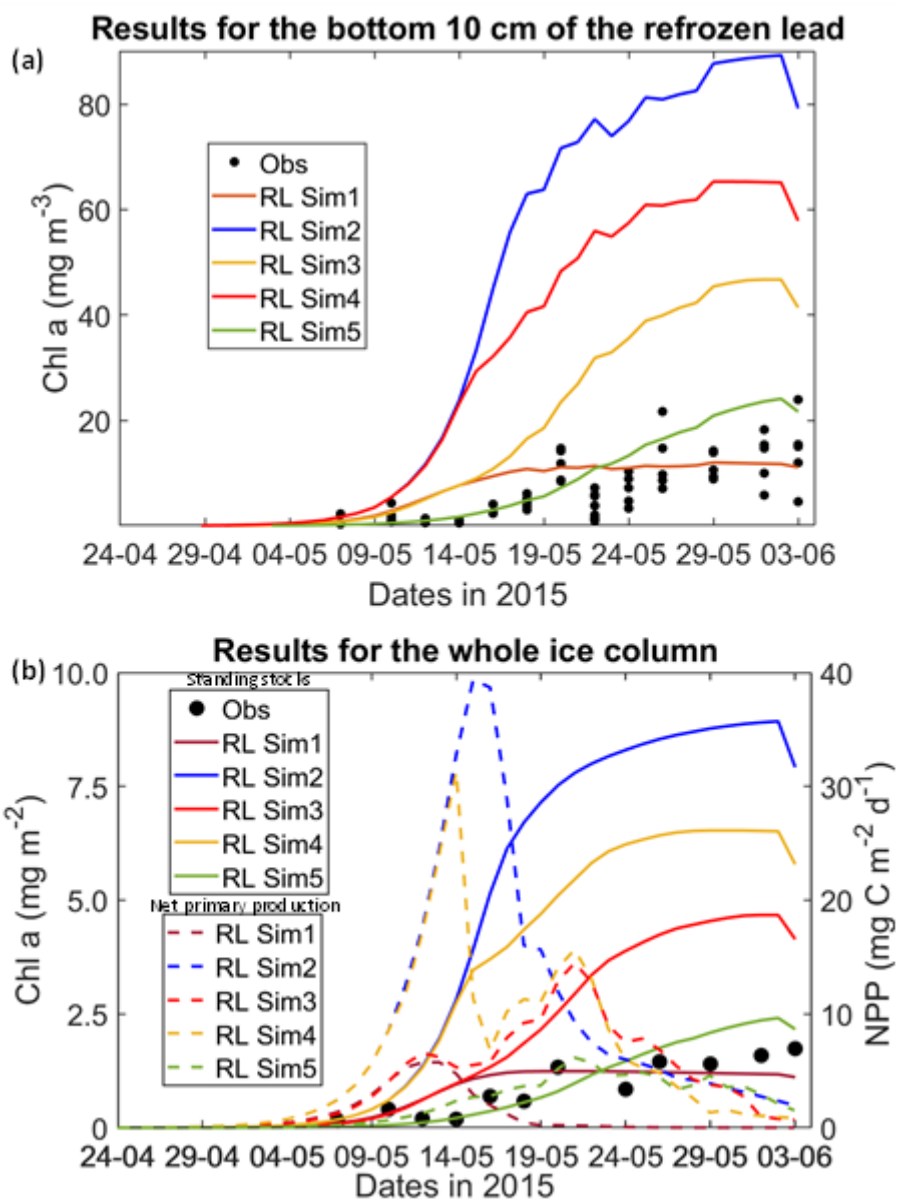
237 map plots) are $< 10 \text{ mg } Chl a \text{ m}^{-3}$. Ice thickness, temperature and salinity profiles are extremely similar among these simulations
238 (Figs. S1 and S2).

239 Results for the silicate and nitrogen limiting factors are based on brine concentrations. Limiting factors exhibiting lower values
240 (more limitation) in RL simulations are silicate, followed by light (Figs. 3, S3 – S5). Limiting values for silicate range between
241 zero (maximum limitation) and one (no limitation), with higher limitation after May 13 in all simulations (Fig. 3). The most
242 severe silicate limitation is for RL_Sim1, where values drop to near zero around middle May. Despite the high average bottom
243 *Chl a* concentration predicted in all simulations the bottom layer is where silicate limitation is less severe after May 13. This
244 is more evident in simulations with turbulent diffusion, where light limitation at the bottom-ice becomes more severe than
245 silicate limitation around the end of May (Fig. S6).

246 Results obtained with RL_Sim6-9, without algal exchanges between the ocean and the ice (see Table 2), show similar patterns
247 of those observed with RL_Sim1-5, respectively (Fig. 4 versus Fig. 2, Fig. S9 versus Fig. 3, Figs. S7 and S8 versus Figs. S1
248 and S2, Figs. S10 – S12 versus Figs. S3 – S5).

249 Interface diffusivity (one of CICE tracers, expressing diffusivity between adjacent biogeochemical layers and between the
250 bottom layers and the ocean) for simulations with turbulent exchanges are up to two orders of magnitude higher at the bottom
251 than for simulations with only molecular diffusion (Fig. 5).

252



253

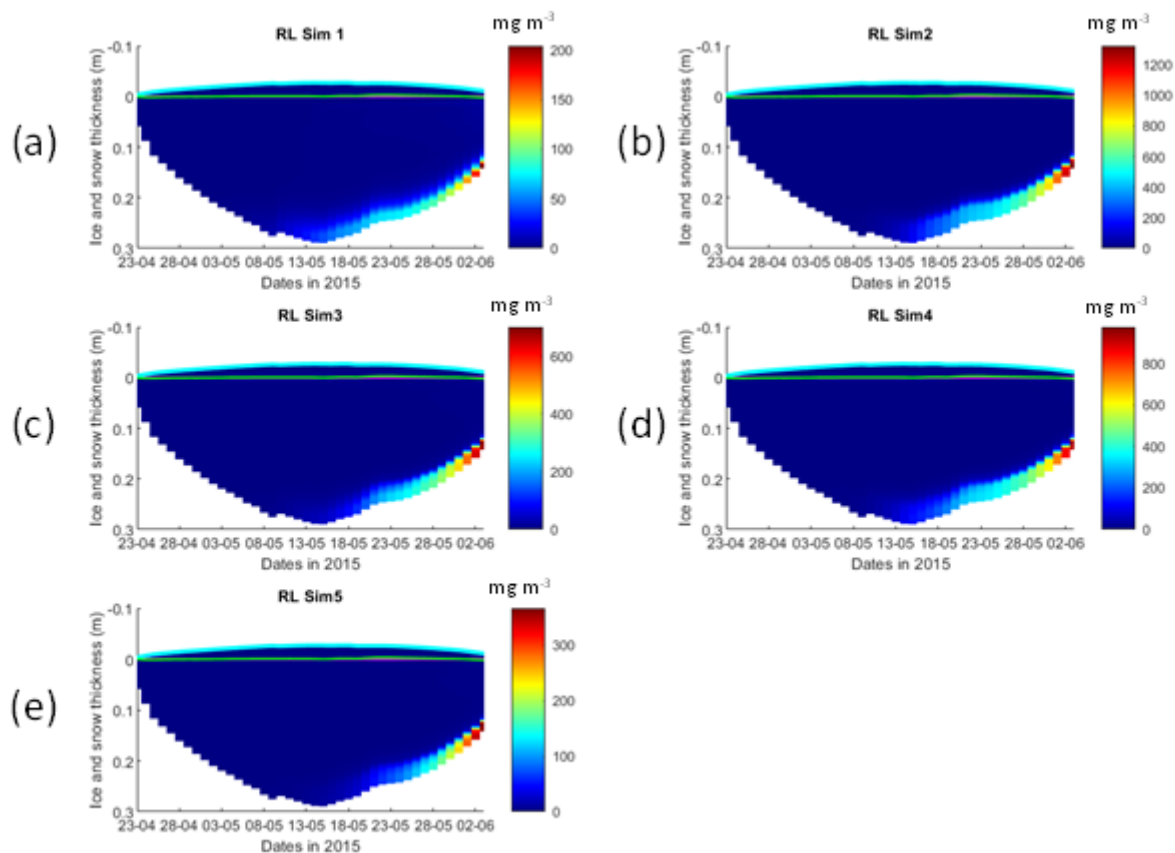
254

255

256

257

Figure 1. Daily averaged results for the refrozen lead (RL): (a) Observed and modelled *Chl a* concentration values averaged for the ice bottom 10 cm; (b) Observed and modelled *Chl a* standing stock (continuous lines) and modelled net primary production (NPP) (dashed lines) for the whole ice column (refer to Table 2 for details about model simulations). Observations are the same presented in Duarte et al. (2017).



258

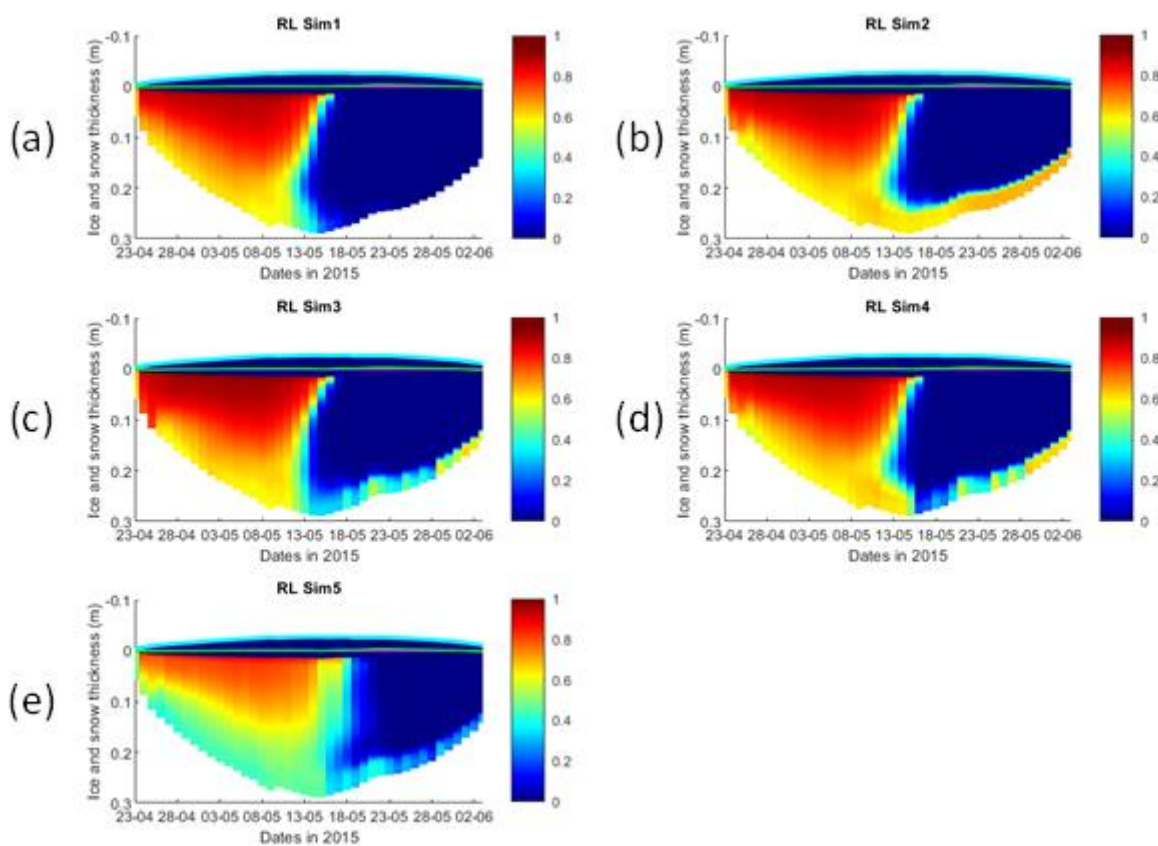
259

260

261

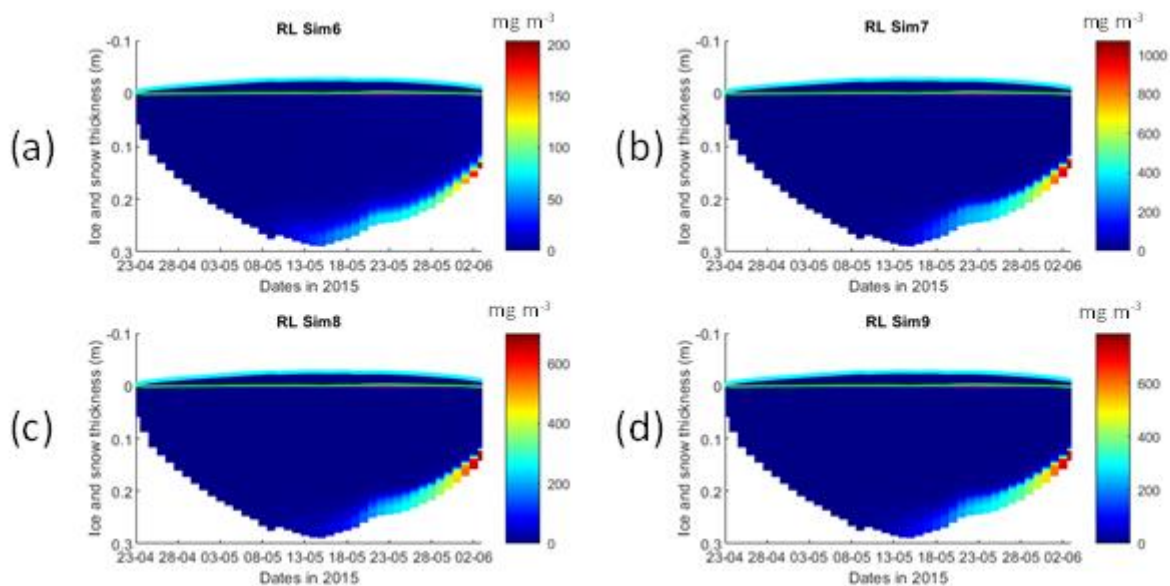
262

Figure 2. Daily averaged results for the refrozen lead (RL) simulations 1 - 5: Simulated evolution of ice algae *Chl a* as a function of time and depth in the ice (note the colour scale differences between the various panels). Ice thickness is given by the distance between the upper and the lower limits of the maps. The upper regions of the graphs, above the green line with zero values, are above the CICE biogrid and have no brine network. The magenta line represents sea level. Refer to Table 2 for details about model simulations.



263

264 **Figure 3. Daily averaged results for the refrozen lead (RL) simulations 1 - 5: Simulated evolution of silicate limitation (one means**
265 **no limitation and zero is maximal limitation), as a function of time and depth in the ice. Ice thickness is given by the distance between**
266 **the upper and the lower limits of the maps. The upper regions of the graphs, above the green line with zero values, are above the**
267 **CICE biogrid and have no brine network. The magenta line represents sea level. Refer to Table 2 for details about model simulations.**



268

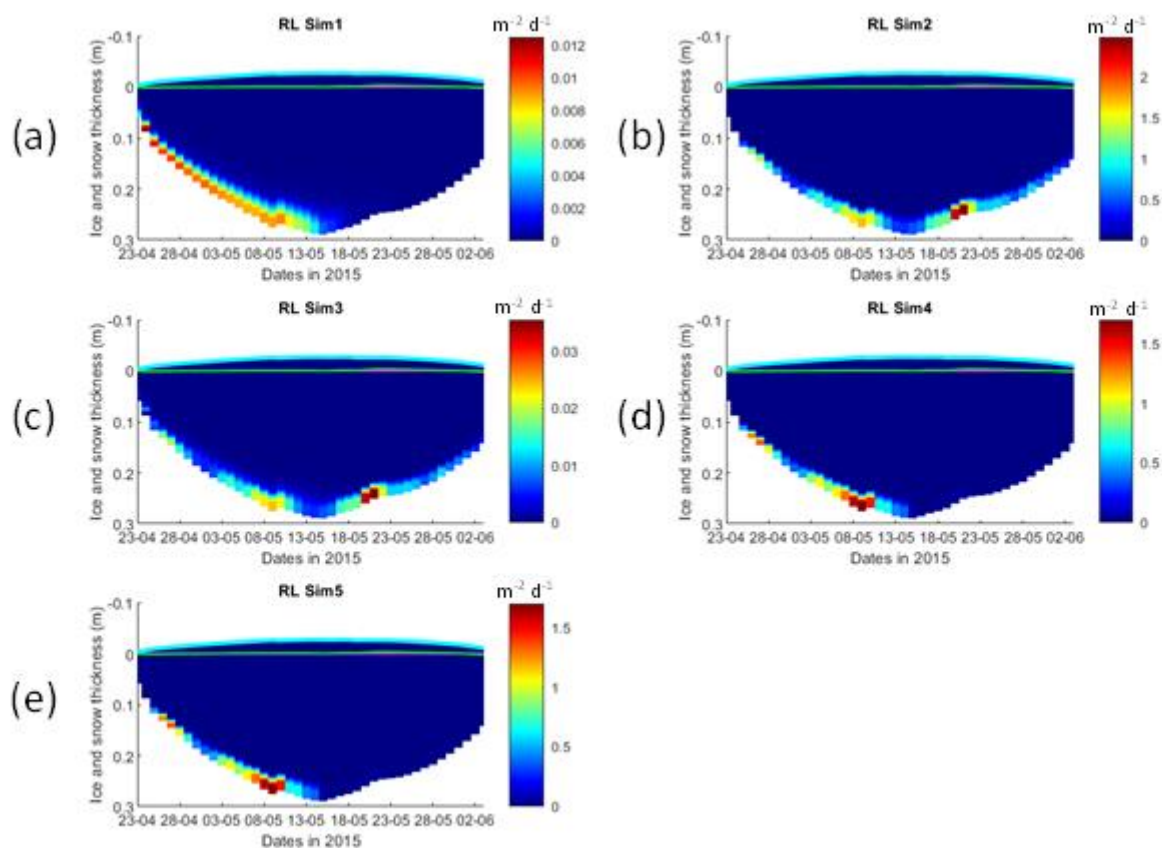
269

270

271

272

Figure 4. Daily averaged results for the refrozen lead (RL) simulations 6 - 9: Simulated evolution of ice algae *Chl a* as a function of time and depth in the ice (note the colour scale differences between the various panels). Ice thickness is given by the distance between the upper and the lower limits of the maps. The upper regions of the graphs, above the green line with zero values, are above the CICE biogrid and have no brine network. The magenta line represents sea level. Refer to Table 2 for details about model simulations.



273

274 **Figure 5. Daily averaged results for the refrozen lead (RL) simulations 1-5: Simulated evolution of interface diffusivity as a function**
275 **of time and depth in the ice (note the colour scale differences between the various panels). Ice thickness is given by the distance**
276 **between the upper and the lower limits of the maps. The upper regions of the graphs, above the green line with zero values, are**
277 **above the CICE biogrid and have no brine network. The magenta line represents sea level. Refer to Table 2 for details about model**
278 **simulations.**

279

280 3.2 Second year ice simulations

281 Simulations with turbulent diffusion (SYI_Sim2 and 3), predict only slightly higher standing stocks and net primary production
282 than with the standard molecular diffusion formulation (SYI_Sim1) (Fig. 6). The visual fit to the standing stock observations
283 is comparable between the various simulations. Changing the half saturation constant for silicate limitation from 2.2 to 4.0 μM
284 has no impact on model results. This is confirmed by analysing the evolution of *Chl a* concentration as a function of time and
285 depth in the ice (Fig. 7), with only minor differences being apparent towards the end of the simulation, when *Chl a* increases



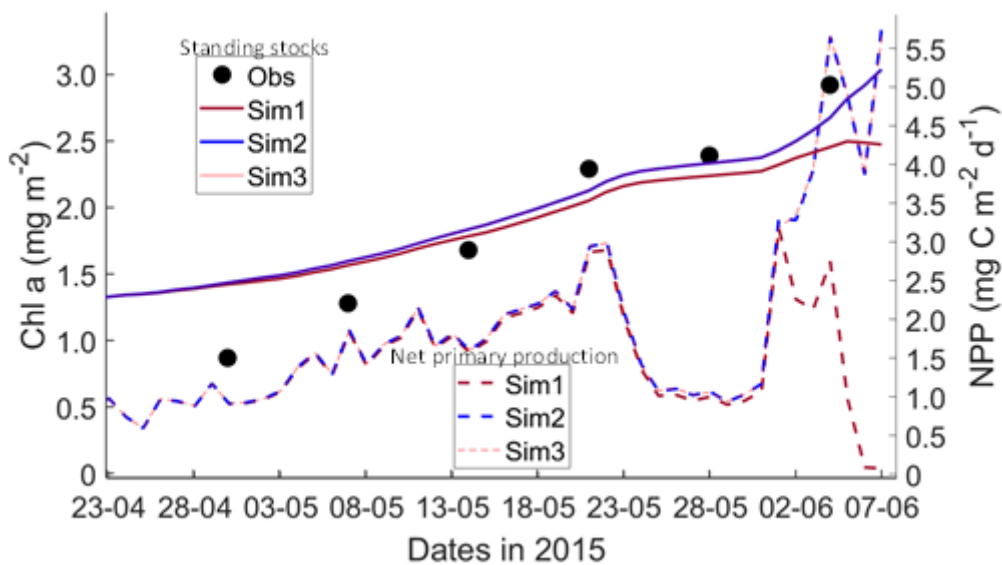
286 at the bottom layers in the simulations with turbulent diffusion (SYI_Sim 2 and 3). Ice thickness, temperature and salinity
287 profiles are extremely similar among these simulations (Fig. S13).

288 The dominant limiting factor in these simulations is light, seconded by silicate (compare Fig. 8a, c and e with 8b, d and f and
289 with Fig. S14). Light limitation is less severe after the onset of snow and ice melting at the beginning of June. Silicate limitation
290 is very strong above the bottom ice. Nitrogen limitation is highest at a depth range between ~0.4 ~0.7 m below the ice top,
291 with a large overlap with the depth range where a *Chl a* maximum is observed (Fig. 7). Maximum *Chl a* values predicted for
292 SYI are between two and three orders of magnitude lower than those predicted for the RL (Figs. 2 and 7). However, standing
293 stocks for the former are larger than those for the latter, considering both observational and model data (Figs. 1b and 6).
294 Opposite to what was described for the RL simulations, silicate limitation becomes more severe than light limitation at the
295 bottom layer only in SYI_Sim_1, at the beginning of June, close to the end of the simulation (Fig. S15).

296 Results obtained without algal exchanges between the ocean and the ice (SYI_Sim4 and 5, see Table 2), show the same patterns
297 of those observed with SYI_Sim1 and 2, respectively (Fig. 9 versus Fig. 7, Fig. S17 versus Fig. 8, Figs. S18 versus S14a - d
298 and Figs. S16 versus S13a - d).

299 Interface diffusivity (one of CICE tracers) for simulations with turbulent exchanges are up to four orders of magnitude higher
300 at the bottom ice than for simulations with only molecular diffusion (Fig. S19, showing a comparison between SYI_Sim1 and
301 SYI_Sim2).

302 SYI_Sim1 and 2 were repeated with varying snow thickness (Table 2 and Figs. 10 and 11). In the former simulation (Fig. 10a),
303 as snow height decreases, there is a reduction in light limitation and a sharp increase in silicate limitation, overtaking light
304 limitation (values becoming lower) as early as mid-May. In the latter simulation (Fig. 10b), light limitation prevails irrespective
305 of snow height, except in the case of the lower snow height of 15 cm where silicate becomes more limiting towards the end of
306 the simulation. With the decrease in snow height, there is an increase in *Chl a* concentration in all simulations. Highest values
307 for SYI_Sim2 are ~one order of magnitude larger than those for SYI_Sim1. Moreover, the decrease in snow heights is followed
308 by an earlier and more intense bottom ice algal bloom.



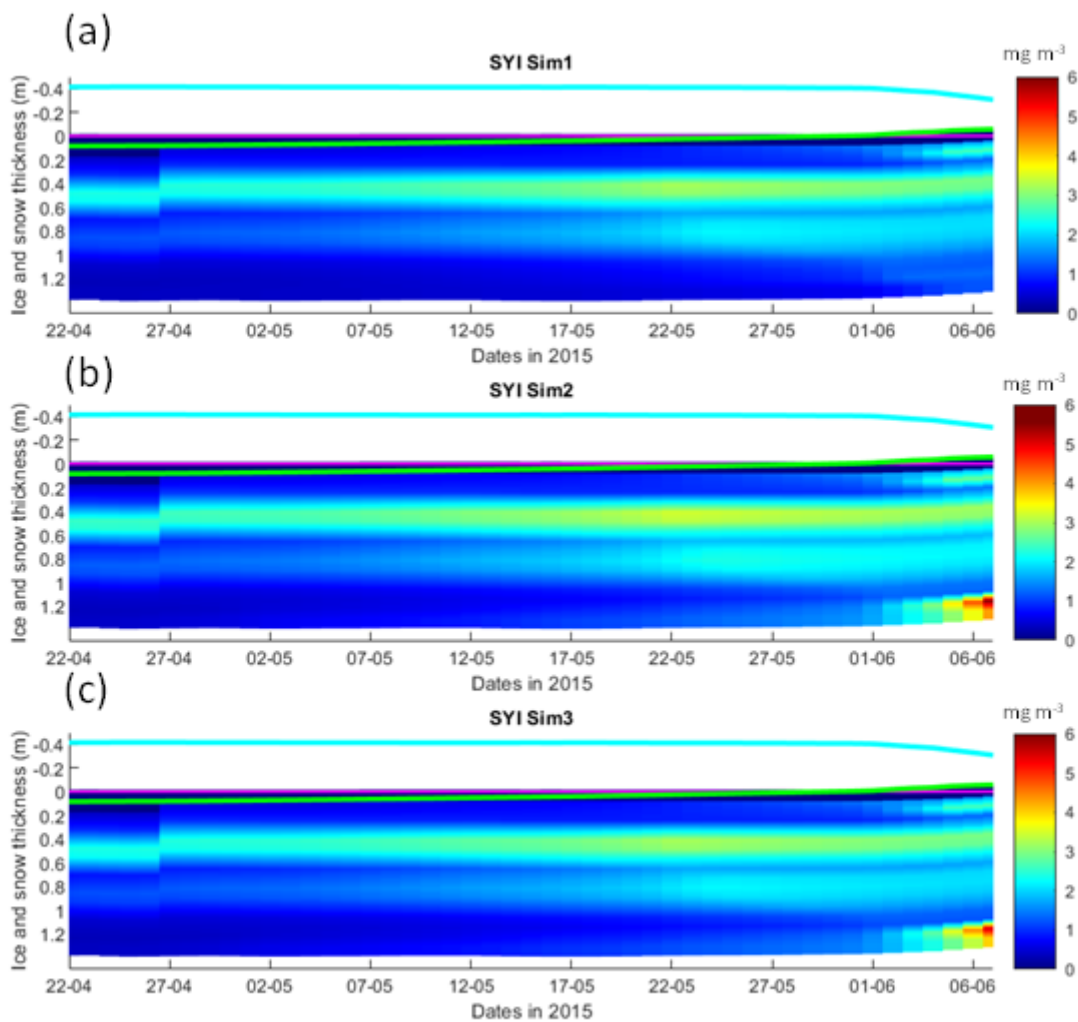
309

310

311

312

Figure 6. Daily averaged results for second year ice (SYI) simulations 1 - 3: Observed [same data presented in Duarte et al. (2017)] and modelled *Chl a* standing stock (continuous lines) and modelled net primary production (NPP) (dashed lines) for the whole ice column (refer to Table 2 for details about model simulations).



313

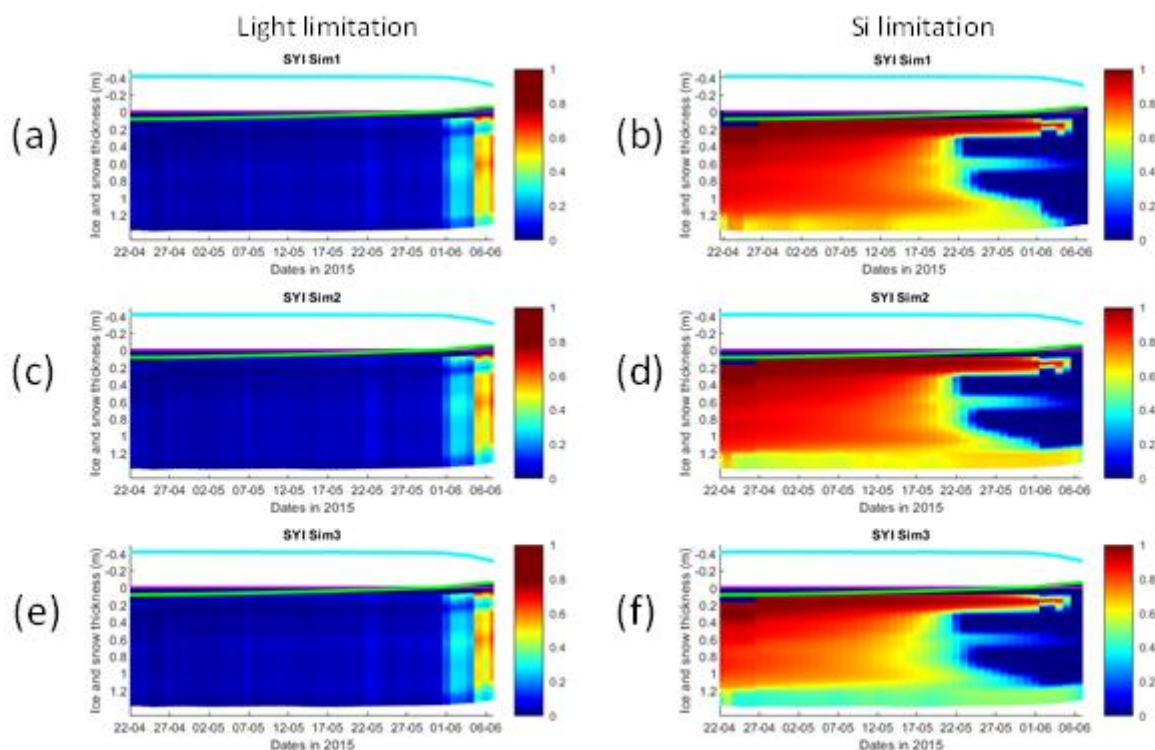
314

315

316

317

Figure 7. Daily averaged results for second year ice (SYI) simulations 1 - 3: Simulated evolution of ice algae *Chl a* as a function of time and depth in the ice. The upper regions of the graphs, above the green line with zero values, are above the CICE biogrid and have no brine network. The magenta line represents sea level, and the cyan line represents the top of the snow layer. Refer to Table 2 for details about model simulations.



318

319

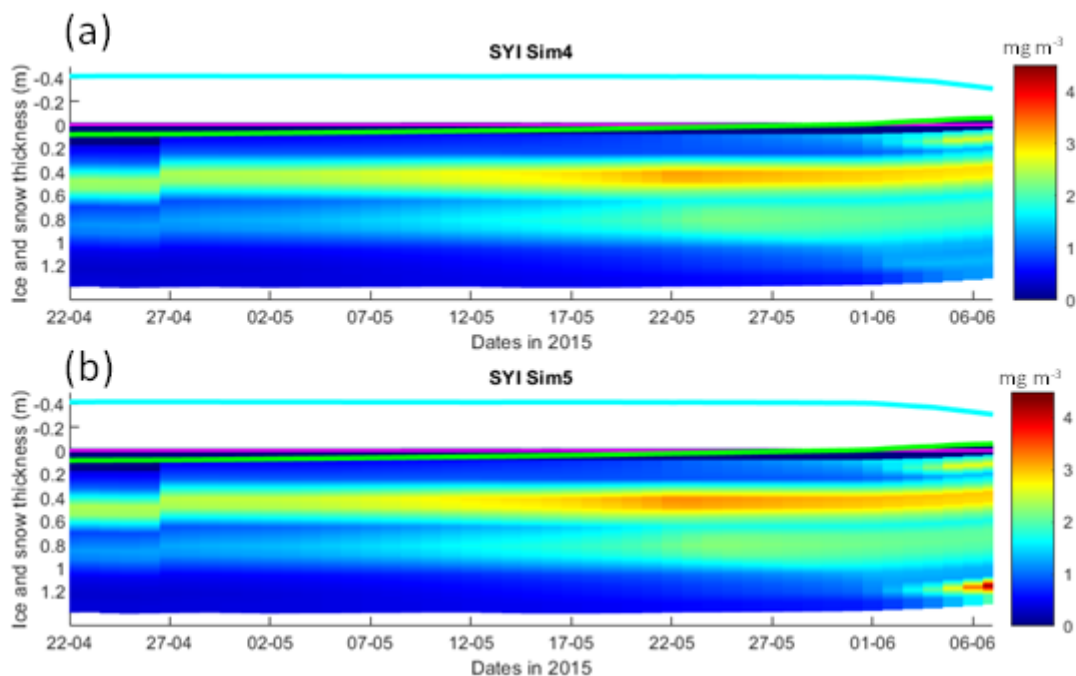
320

321

322

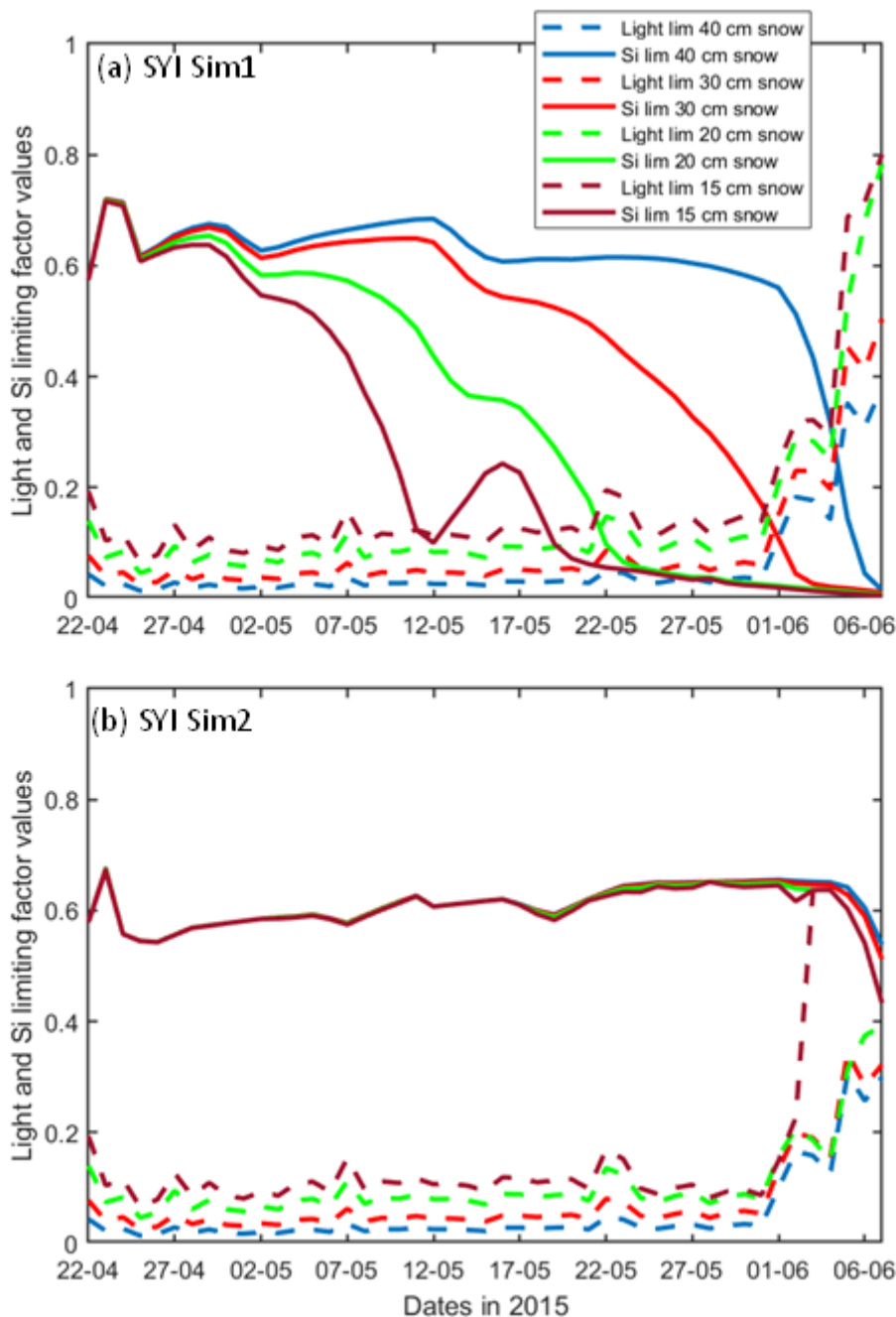
323

Figure 8. Daily averaged results for second year ice (SYI) simulations 1 - 3: Simulated evolution of light (left panels) and silicate (right panels) limitation (one means no limitation and zero is maximal limitation), as a function of time and depth in the ice. The upper regions of the graphs, above the green line with zero values, are above the CICE biogrid and have no brine network. The magenta line represents sea level, and the cyan line represents the top of the snow layer. Refer to Table 2 for details about model simulations.



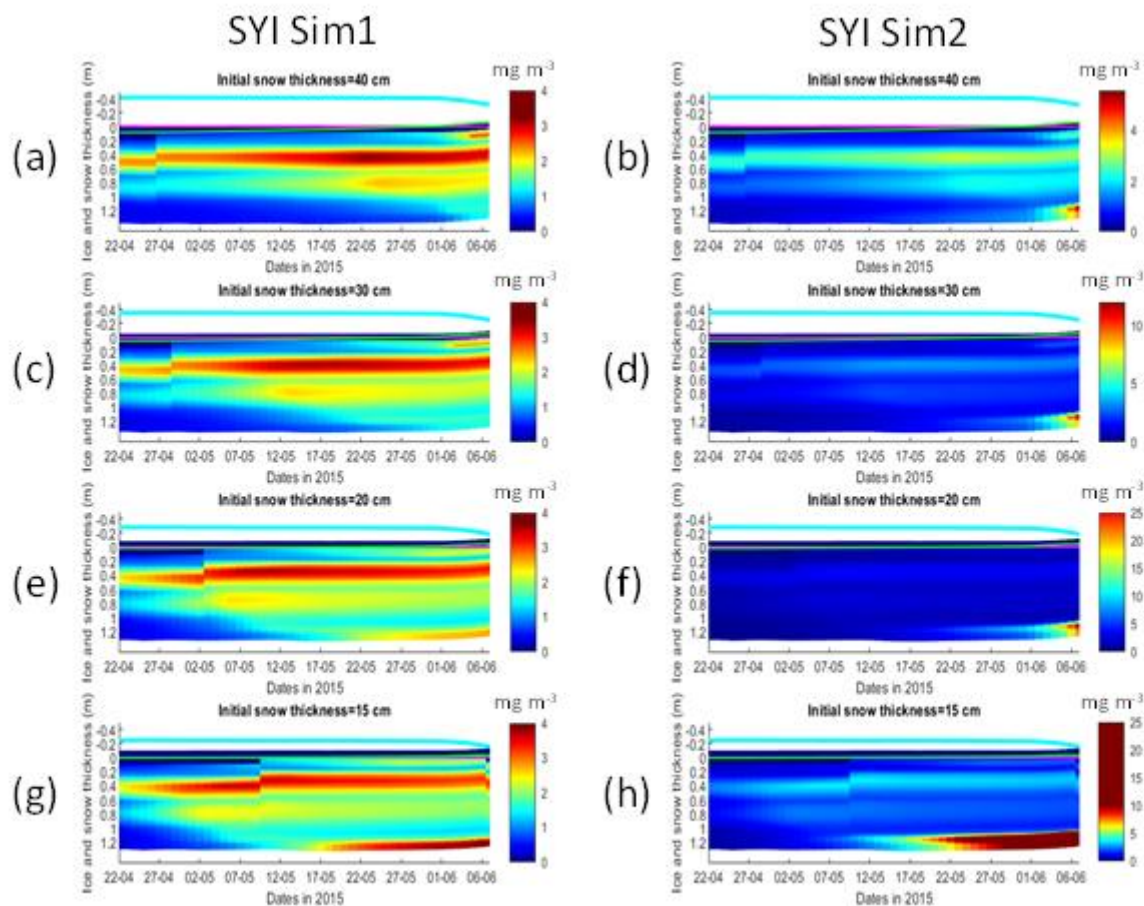
324
325
326
327
328

Figure 9. Daily averaged results for second year ice (SYI) simulations 4 and 5: Simulated evolution of ice algae *Chl a* as a function of time and depth in the ice. The upper regions of the graphs, above the green line with zero values, are above the CICE biogrid and have no brine network. The magenta line represents sea level, and the cyan line represents the top of the snow layer. Refer to Table 2 for details about model simulations.



329

330 **Figure 10.** Daily averaged results for the second-year ice (SYI) simulations 1 (a) and 2 (b) starting with a snow depth of 40 (default
331 simulation), 30, 20 and 15 cm: Simulated evolution of light (dashed lines) and silicate (continuous lines) limitation (one means no
332 limitation and zero is maximal limitation), as a function of time at the ice bottom layer (one means no limitation). Refer to Table 2
333 for details about model simulations.



334

335 **Figure 11.** Daily averaged results for second year ice (SYI) simulations 1 (left panels) and 2 (right panels) starting with a snow depth
336 of 40 (default simulation), 30, 20 and 15 cm: Simulated evolution of ice algae *Chl a* as a function of time and depth in the ice. The
337 upper regions of the graphs, above the green line with zero values, are above the CICE biogrid and have no brine network. The
338 magenta line represents sea level, and the cyan line represents the top of the snow layer. Refer to Table 2 for a description of model
339 simulations.

340 4. Discussion

341 The results obtained in this study support the initial hypothesis, showing that replacing molecular with turbulent diffusion at
342 the ice-ocean interface, formulated in a way consistent with momentum and heat exchanges, leads to a reduction in nutrient
343 limitation that supports a significant increase in ice algal net primary production and *Chl a* biomass accumulation in the bottom
344 ice layers, when production is understood to be nutrient limited.



345 The implementation of turbulent mixing considerably relieved silicate limitation in the RL simulations, leading to an increase
346 in bottom *Chl a* concentration and in-ice light absorption, increasing light limitation due to shelf-shading [in the CICE model,
347 optical ice properties are influenced by ice algal concentrations (Jeffery et al., 2016)].

348 In the N-ICE2015 biogeochemical dataset (Assmy et al., 2016), the median of dissolved inorganic nitrogen to silicate ratios in
349 all surface and subsurface water masses, is above 1.7 (unpublished data), which is the upper limit for the nitrogen to silicate
350 ratio for polar diatoms (e.g. Takeda, 1998; Krause et al. 2018). Therefore, it can be expected that, in the region covered by the
351 N-ICE2015 expedition, silicate is more limiting than nitrogen for the production yields of the pennate diatoms characteristic
352 of the bottom-ice communities [the dominant algal functional group in bottom ice, e.g. Leu et al. (2015), van Leeuwe et al.
353 (2019)]. Elsewhere in the Arctic the opposite may be true, considering nitrate and silicate concentrations presented in Leu et
354 al. (2015) and the number of process studies documenting such limitation (e.g. Campbell et al. 2016). However, the conclusions
355 taken here about the effects of turbulent mixing are independent of the limiting nutrient.

356 Implementing turbulent diffusion has obvious implications for model tuning. Our results for the RL show that with this
357 formulation it was necessary to increase the half saturation constant for silicate uptake and to reduce the ocean concentration
358 of algal nitrogen (algalN), reducing the colonization of bottom ice by ice algae, to obtain *Chl a* values comparable to those
359 observed (RL_Sim5). Therefore, whereas Duarte et al. (2017) had to reduce silicate limitation to improve the fit between
360 modelled and observational data, the opposite approach was required when using turbulent diffusion. This is an example of
361 how one can get good model results by the wrong reasons with difficult to predict consequences on model forecasts under
362 various scenarios.

363 In the SYI case, only a minor increase in bottom *Chl a* concentration was observed towards the end of simulations SYI_Sim_2
364 and SYI_Sim_3, when light limitation due to the thick snow cover was relieved by snow melt. Silicate limitation was not as
365 severe as in SYI_Sim_1, due to greater bottom exchanges in the former simulations. The importance of snow cover in
366 controlling ice algal phenology has been stressed before [e.g., Campbell et al. (2015), Leu et al. (2015)].

367 Duarte et al. (2017) used the delta-Eddington parameter, corresponding to the standard deviation of the snow grain size
368 (R_{snow}) (Urrego-Blanco et al., 2016), to tune model predicted shortwave radiation at the ice bottom. However, there was
369 still a positive model bias in June. Therefore, our conclusion about the main limiting role of light in SYI is conservative.
370 Moreover, in part of SYI cores sampled during the N-ICE2015 expedition, in the period covered by our simulations, with an
371 unusually high snow thickness (~40 cm), there was no *Chl a* bottom maximum (Duarte et al., 2017; Olsen et al., 2017).

372 The dominant role of light limitation in SYI was confirmed in the simulations with reduced snow thickness and alleviated light
373 limitation, with a bottom-ice algal *Chl a* maximum emerging earlier at snow thickness ≤ 20 cm. The reduction of snow heights
374 had a much larger effect in increasing *Chl a* concentration at the bottom layer when turbulent mixing was used, due to lower
375 silicate limitation. Reducing snow height led to a relatively early shift from light to silicate limitation when we used molecular
376 diffusion, whereas this shift occurred only at the very end of the simulated period when we used turbulent diffusion. The effects
377 of molecular versus turbulent diffusion, upon reduction of the snow cover and the possible development of a bottom ice algal



378 bloom, are critical aspects when simulating ice algal phenology and attempting to quantify the contribution of sympagic algae
379 to Arctic primary production.

380 Simulated turbulent diffusivities are up to four orders of magnitude higher than molecular diffusivities and the results presented
381 herein emphasize their potential role in sea ice biogeochemistry. The number and intensity of Arctic winter storms has
382 increased over the 1979–2016 period (Rinke et al., 2017; Graham et al., 2017) and the effect of more frequent and more
383 intensive winter storms in the Atlantic Sector of the Arctic Ocean is a thinner, weaker, and younger snow-laden ice pack
384 (Graham et al., 2019). Storms that occur late in the winter season, after a deep snowpack has accumulated, have the potential
385 to promote ice growth by dynamically opening leads where new ice growth can take place. The young ice of the refrozen leads
386 does not have time to accumulate a deep snow layer until the melting season, which could lead to light limitation of algal
387 growth. All things considered, it can be expected that ongoing trends in the Arctic will lead to a release from light limitation
388 in increasingly larger areas of the ice pack in late winter, which will lead to more likely nutrient limitation earlier in spring
389 (e.g. Lannuzel et al. 2020). These effects will be further amplified under thinning of the snowpack as observed in western
390 Arctic, and in the Beaufort and Chukchi seas, over the last decades (Webster et al., 2014). Therefore, properly parameterizing
391 nutrient exchanges between the ice and the ocean in sea-ice biogeochemical models is of utmost importance to avoid
392 overestimating nutrient limitation and thus underestimating sea ice algal primary production.

393 In existing sea-ice models there are “natural” differences between the way budgets for non-conservative tracers such as
394 nutrients are closed compared to those of momentum, heat and salt, which are related to the biogeochemical sinks and sources
395 (e.g., equation 18 in Vancoppenolle et al., 2010), but also some “inconsistencies”, related with the way their transfers between
396 the ocean and the ice are computed. Interestingly, some models (e.g., Jin et al., 2006, 2008 and Hunke et al., 2016) apply the
397 diffusion equation to calculate exchanges across the bottom ice not only to dissolved tracers, but also to algal cells. This is to
398 guarantee a mechanism of ice colonization by microalgae. However, the usage of the same coefficient for dissolved and
399 particulate components creates significant uncertainty.

400 Molecular diffusion is a slow process compared with momentum and heat turbulent exchanges. This justifies the usage of
401 diffusion coefficients which are much higher than molecular diffusivity, as in Jin et al. (2006), using a value of $1.0 \times 10^{-5} \text{ m}^2$
402 s^{-1} , four orders of magnitude higher than the value indicated in Mann and Lazier (2005) – $1.5 \times 10^{-9} \text{ m}^2 \text{ s}^{-1}$ – or the
403 parameterization of diffusivity as a function of friction velocity as in Mortenson et al. (2017). The approach proposed herein,
404 formulating bottom-ice nutrient exchanges in a way that is consistent with momentum and heat exchanges, provides a
405 physically sound, consistent, and easy to implement alternative.

406 5. Conclusions

407 Replacing molecular with turbulent diffusion at the ice-ocean interface in a sea-ice biogeochemical sub-model, leads to a
408 reduction in nutrient limitation and a significant increase in ice algal net primary production and *Chl a* biomass accumulation
409 in the bottom-ice layers, when production is nutrient limited. The results presented herein emphasize the potential role of



410 bottom-ice nutrient exchange processes, irrespective of brine dynamics and other physical-chemical processes, in delivering
411 nutrients to bottom-ice algal communities, and thus the importance of properly including them in sea-ice models. The relevance
412 of this becomes even more apparent considering ongoing changes in the Arctic icescape, with a predictable decrease in light
413 limitation as ice becomes thinner and more fractured, with an expected reduction in snow cover.

414 **Code availability**

415 The software code used in this study may be found at:

416 <https://doi.org/10.5281/zenodo.4675097> and <https://doi.org/10.5281/zenodo.4675021>

417 This code is in a fork derived from the CICE Consortium repository (<https://github.com/CICE-Consortium>).

418 The Consortium's codes are open-source with a standard 3-clause BSD license and are under the following Copyright
419 license, available at (<https://cice-consortium-cice.readthedocs.io/en/master/intro/copyright.html>):

420

421 **Data availability**

422 Model forcing function files may be found at: <https://doi.org/10.5281/zenodo.4672176>

423 Results from model simulations described above, in the form of CICE daily netCDF history files iceh.* may be found at:

424 <http://doi.org/10.5281/zenodo.4672210>

425 There is one directory for each simulation, and it includes besides the historical files the input file (ice_in) with the simulation
426 parameters.

427

428 **Authors contribution**

429 Pedro Duarte made the software changes, designed the experiments, performed the simulations and prepared the manuscript
430 with contributions from all co-authors.

431 Philipp Assmy contributed to the writing of the manuscript.

432 Karley Campbell contributed to the writing of the manuscript.

433 Arild Sundfjord contributed to the writing of the manuscript and to funding acquisition.

434

435 **Competing interests**

436 The authors declare that they have no conflict of interest.

437 **Acknowledgements**

438 This work has been supported by the Fram Centre Arctic Ocean flagship project "Mesoscale physical and biogeochemical
439 modelling of the ocean and sea-ice in the Arctic Ocean" (project reference 66200), the Norwegian Metacenter for



440 Computational Science application “NN9300K - Ecosystem modelling of the Arctic Ocean around Svalbard”, the Norwegian
441 “Nansen Legacy” project (no. 276730) and the European Union’s Horizon 2020 research and innovation programme under
442 grant agreement No 869154. Contributions by K Campbell are supported by the Diatom ARCTIC project
443 (NE/R012849/1;03F0810A), part of the Changing Arctic Ocean program, jointly funded by the UKRI Natural Environment
444 Research Council and the German Federal Ministry of Education and Research (BMBF).

445 **References**

- 446 Arrigo, K. R., Kremer, J. N., and Sullivan, C. W.: A Simulated Antarctic Fast Ice Ecosystem, *J. Geophys. Res.*, 98, 17, 1993.
- 447 Assmy, P., Duarte, P., Dujardin, J., Fernández-Méndez, M., Fransson, A., Hodgson, R., Kauko, H., Kristiansen, S., Mundy, C.
448 J., Olsen, L. M., Peeken, I., Sandbu, M., Wallenschus, J., Wold, A.: N-ICE2015 water column biogeochemistry [Data set],
449 Norwegian Polar Institute, <https://doi.org/10.21334/npolar.2016.3ebb7f64>, 2017.
- 450 Assmy, P., Dodd, P. A., Duarte, P., Dujardin, J., Elliott, A., Fernández-Méndez, M., Fransson, A., Granskog, M. A., Hendry,
451 K., Hodgson, R., Kauko, H., Kristiansen, S., Leng, M. J., Meyer, A., Mundy, C. J., Olsen, L. M., Peeken, I., Sandbu, M.,
452 Wallenschus, J., Wold, A.: N-ICE2015 sea ice biogeochemistry [Data set], Norwegian Polar Institute,
453 <https://doi.org/10.21334/npolar.2017.d3e93b31>, 2017.
- 454 Brzezinski, M. A.: The Si-C-N Ratio of Marine Diatoms - Interspecific Variability and the Effect of Some Environmental
455 Variables, *J. Phycol.*, 21, 347-357, 1985.
- 456 Campbell, K., Mundy, C. J., Barber, D. G. and Gosselin, M.: Characterizing the sea ice algae chlorophyll a–snow depth
457 relationship over Arctic spring melt using transmitted irradiance, *J. Mar. Sys.*, 147, 76-84, doi:
458 <https://doi.org/10.1016/j.jmarsys.2014.01.008>, 2015.
- 459 Campbell, K., Mundy, C. J., Landy, J. C., Delaforge, A., Michel, C. and Rysgaard, S.: Community dynamics of bottom-ice
460 algae in Dease Strait of the Canadian Arctic. *Prog. Oceanogr.*, 149, 27-39, doi: <http://dx.doi.org/10.1016/j.pocean.2016.10.005>,
461 2016.
- 462 Carmack, E.: Circulation and Mixing in Ice-Covered Waters, in: *The Geophysics of Sea Ice. NATO ASI Series (Series B:
463 Physics)*, edited by Untersteiner N. Springer, Boston, MA. 641-712, https://doi.org/10.1007/978-1-4899-5352-0_11, 1986.
- 464 Cota, G. F., Prinsenberg, S. J., Bennett, E. B., Loder, J. W., Lewis, M. R., Anning, J. L., Watson, N. H. F., and Harris, L. R.:
465 Nutrient Fluxes during Extended Blooms of Arctic Ice Algae, *J. Geophys. Res.-Oceans*, 92, 1951-1962, doi:
466 10.1029/Jc092ic02p01951, 1987.
- 467 Cota, G. F., and Horne, E. P. W.: Physical Control of Arctic Ice Algal Production, *Mar. Ecol. Prog. Ser.*, 52, 111-121, doi:
468 10.3354/meps052111, 1989.
- 469 Cota, G. F., and Sullivan, C. W.: Photoadaptation, Growth and Production of Bottom Ice Algae in the Antarctic, *J. Phycol.*,
470 26, 399-411, doi: 10.1111/j.0022-3646.1990.00399.x, 1990.



- 471 Dalman, L. A., Else, B. G. T., Barber, D., Carmack, E., Williams, W. J., Campbell, K., Duke, P. J., Kirillov, S., and Mundy,
472 C. J.: Enhanced bottom-ice algal biomass across a tidal strait in the Kitikmeot Sea of the Canadian Arctic, *Elem. Sci. Anth.*, 7,
473 doi: <https://doi.org/10.1525/elementa.361>, 2019.
- 474 Duarte, P., Meyer, A., Olsen, L. M., Kauko, H. M., Assmy, P., Rosel, A., Itkin, P., Hudson, S. R., Granskog, M. A., Gerland,
475 S., Sundfjord, A., Steen, H., Hop, H., Cohen, L., Peterson, A. K., Jeffery, N., Elliott, S. M., Hunke, E. C., and Turner, A. K.:
476 Sea ice thermohaline dynamics and biogeochemistry in the Arctic Ocean: Empirical and model results, *J. Geophys. Res.-*
477 *Biogeosciences*, 122, 1632-1654, doi: 10.1002/2016JG003660, 2017.
- 478 Duarte, P.: CICE-Consortium/Icepack: Icepack with bottom drag, heat and nutrient turbulent diffusion (Version 1.1). Zenodo.
479 <http://doi.org/10.5281/zenodo.4675021>, (2021a, April 9).
- 480 Duarte, P.: CICE-Consortium/CICE: CICE with bottom drag, heat and nutrient turbulent diffusion (Version 1.1). Zenodo.
481 <http://doi.org/10.5281/zenodo.4675097>, (2021b, April 9).
- 482 Duarte, P.: The importance of turbulent ocean-sea ice nutrient exchanges for simulation of ice algal biomass and production
483 with CICE6.1 and Icepack 1.2 - CICE forcing files (Version v1.0) [Data set]. Zenodo. <http://doi.org/10.5281/zenodo.4672176>,
484 2021c.
- 485 Duarte, P.: The importance of turbulent ocean-sea ice nutrient exchanges for simulation of ice algal biomass and production
486 with CICE6.1 and Icepack 1.2 - model simulations (Version v1.0) [Data set]. Zenodo. <http://doi.org/10.5281/zenodo.4672210>,
487 2021c.
- 488 Gerland, S., Granskog, M. A., King, J., Rösel, A.: N-ICE2015 Ice core physics: temperature, salinity and density [Data set],
489 Norwegian Polar Institute, <https://doi.org/10.21334/npolar.2017.c3db82e3>, 2017.
- 490 Gosselin, M., Legendre, L., Demers, S., and Ingram, R. G.: Responses of Sea-Ice Microalgae to Climatic and Fortnightly Tidal
491 Energy Inputs (Manitounuk Sound, Hudson-Bay), *Can. J. Fish. Aquat. Sci.*, 42, 999-1006, doi: 10.1139/f85-125, 1985.
- 492 Graham, R. M., Rinke, A., Cohen, L., Hudson, S. R., Walden, V. P., Granskog, M. A., Dorn, W., Kayser, M., and Maturilli,
493 M.: A comparison of the two Arctic atmospheric winter states observed during N-ICE2015 and SHEBA, *J. Geophys. Res.-*
494 *Atmospheres*, 122, 5716-5737, doi: 10.1002/2016JD025475, 2017.
- 495 Graham, R. M., Itkin, P., Meyer, A., Sundfjord, A., Spreen, G., Smedsrud, L. H., Liston, G. E., Cheng, B., Cohen, L., Divine,
496 D., Fer, I., Fransson, A., Gerland, S., Haapala, J., Hudson, S. R., Johansson, A. M., King, J., Merkouriadi, I., Peterson, A. K.,
497 Provost, C., Randelhoff, A., Rinke, A., Rosel, A., Sennechael, N., Walden, V., Duarte, P., Assmy, P., Steen, H., and Granskog,
498 M. A.: Winter storms accelerate the demise of sea ice in the Atlantic sector of the Arctic Ocean, *Sci. Rep.-Uk*, 9, Artn 9222,
499 doi: 10.1038/S41598-019-45574-5, 2019.
- 500 Granskog, M. A., Fer, I., Rinke, A., and Steen, H.: Atmosphere-Ice-Ocean-Ecosystem Processes in a Thinner Arctic Sea Ice
501 Regime: The Norwegian Young Sea ICE (N-ICE2015) Expedition, *J. Geophys. Res.-Oceans*, 123, 1586-1594, doi:
502 10.1002/2017jc013328, 2018.
- 503 Hegseth, E. N.: Sub-Ice Algal Assemblages of the Barents Sea - Species Composition, Chemical-Composition, and Growth-
504 Rates, *Polar. Biol.*, 12, 485-496, 1992.



- 505 Hudson, S. R., Cohen, L., Walden, V.: N-ICE2015 surface meteorology [Data set], Norwegian Polar Institute,
506 <https://doi.org/10.21334/npolar.2015.056a61d1>, 2015.
- 507 Hudson, S. R., Cohen, L., Walden, V.: N-ICE2015 surface broadband radiation data [Data set], Norwegian Polar Institute,
508 <https://doi.org/10.21334/npolar.2016.a89cb766>, 2016.
- 509 Hunke, E. C., Lipscomb, W. H., Turner, A. K., Jeffery, N., Elliot, S.: CICE: the Los Alamos Sea Ice Model. Documentation
510 and User's Manual Version 5.1. Los Alamos National Laboratory, USA. LA-CC-06-012, 2015.
- 511 Ingram, R. G., Osler, J. C., and Legendre, L.: Influence of Internal Wave-Induced Vertical Mixing on Ice Algal Production in a
512 Highly Stratified Sound, *Estuar. Coast. Shelf. S.*, 29, 435-446, doi: 10.1016/0272-7714(89)90078-4, 1989.
- 513 Jeffery, N., Hunke, E. C., and Elliott, S. M.: Modeling the transport of passive tracers in sea ice, *J. Geophys. Res.-Oceans*,
514 116, Artn C07020, doi:10.1029/2010jc006527, 2011.
- 515 Jeffery, N., Elliott, S., Hunke, E. C., Lipscomb, W. H., Turner, A. K.: Biogeochemistry of CICE: The Los Alamos Sea Ice
516 Model, Documentation and User's Manual. Zbgc_colpkg modifications to Version 5, Los Alamos National Laboratory, Los
517 Alamos, N. M., 2016.
- 518 Jin, M., Deal, C. J., Wang, J., Shin, K. H., Tanaka, N., Whitley, T. E., Lee, S. H., and Gradinger, R. R.: Controls of the
519 landfast ice-ocean ecosystem offshore Barrow, Alaska, *Ann. Glaciol.*, 44, 9, 2006.
- 520 Jin, M., Deal, C., and Jia, W.: A coupled ice-ocean ecosystem model for I-D and 3-D applications in the Bering and Chukchi
521 Seas, *Chinese Journal of Polar Science*, 19, 11, 2008.
- 522 Krause, J. W., Duarte, C. M., Marquez, I. A., Assmy, P., Fernandez-Mendez, M., Wiedmann, I., Wassmann, P., Kristiansen,
523 S., and Agusti, S.: Biogenic silica production and diatom dynamics in the Svalbard region during spring, *Biogeosciences*, 15,
524 6503-6517, doi: 10.5194/bg-15-6503-2018, 2018.
- 525 Lake, R. A., Lewis, E. L.: Salt rejection by sea ice during growth, *J. Geophys. Res.*, 75, 583-597, 1970.
- 526 Lannuzel, D., Tedesco, T., van Leeuwe, M., Campbell, K., Flores, H., Delille, B., Miller, L., Stefels, J., Assmy, P., Bowman,
527 J., Brown, K., Castellani, G., Chierici, M., Crabeck, O., Damm, E., Else, B., Fransson, A., Fripiat, F., Geilfus, N. X., Jacques,
528 C., Jones, E., Kaartokallio, H., Kotovitch, M., Meiners, K., Moreau, S., Nomura, D., Peeken, I., Rintala, J. M., Steiner, N.,
529 Tison, J. L., Vancoppenolle, M., Van der Linden, F., Vichi, M. and Wongpan, P.: The future of Arctic sea-ice biogeochemistry
530 and ice-associated ecosystems, *Nat. Clim. Change* 10(11), 983-992, doi: <https://doi.org/10.1038/s41558-020-00940-4>, 2020.
- 531 Lavoie, D., Denman, K., and Michel, C.: Modeling ice algal growth and decline in a seasonally ice-covered region of the
532 Arctic (Resolute Passage, Canadian Archipelago), *J. Geophys. Res.-Oceans*, 110, Artn C11009, doi: 10.1029/2005jc002922,
533 2005.
- 534 Leu, E., Mundy, C. J., Assmy, P., Campbell, K., Gabrielsen, T. M., Gosselin, M., Juul-Pedersen, T., and Gradinger, R.: Arctic
535 spring awakening - Steering principles behind the phenology of vernal ice algal blooms, *Progr. Oceanogr.*, 139, 151-170, doi:
536 10.1016/j.pocean.2015.07.012, 2015.
- 537 Mann, K. H., Lazier, J. R. N.: *Dynamics of Marine Ecosystems*, Third Edition, Blackwell Publishing Ltd., Carlton, Victoria
538 3053, Australia, 503p., doi:10.1002/9781118687901, 2005.



- 539 McPhee, M.: Air-ice-ocean interaction: Turbulent ocean boundary layer exchange processes. Springer-Verlag, New York,
540 216p., doi: 10.1007/978-0-387-78335-2, 2008.
- 541 McPhee, M. G., Morison, J. H., and Nilsen, F.: Revisiting heat and salt exchange at the ice-ocean interface: Ocean flux and
542 modeling considerations, *J. Geophys. Res.-Oceans*, 113, Artn C06014, doi: 10.1029/2007jc004383, 2008.
- 543 Mortenson, E., Hayashida, H., Steiner, N., Monahan, A., Blais, M., Gale, M. A., Galindo, V., Gosselin, M., Hu, X. M., Lavoie,
544 D., and Mundy, C. J.: A model-based analysis of physical and biological controls on ice algal and pelagic primary production
545 in Resolute Passage, *Elem. Sci. Anth.*, 5, Artn 39, doi:10.1525/Elementa.229, 2017.
- 546 Nelson, D. M., and Treguer, P.: Role of Silicon as a Limiting Nutrient to Antarctic Diatoms - Evidence from Kinetic-Studies
547 in the Ross Sea Ice-Edge Zone, *Mar. Ecol. Prog. Ser.*, 80, 255-264, doi: 10.3354/meps080255, 1992.
- 548 Niedrauer, T. M., and Martin, S.: Experimental-Study of Brine Drainage and Convection in Young Sea Ice, *J. Geophys. Res.-*
549 *Oceans*, 84, 1176-1186, doi: 10.1029/JC084iC03p01176, 1979.
- 550 Olsen, L. M., Laney, S. R., Duarte, P., Kauko, H. M., Fernández-Méndez, M., Mundy, C. J., Rösel, A., Meyer, A., Itkin, P.,
551 Cohen, L., Peeken, I., Tatarek, A., Róžańska, M., Wiktor, J., Taskjelle, T., Pavlov, A. K., Hudson, S. R., Granskog, M. A.,
552 Hop, H., and Assmy, P.: The seeding of ice-algal blooms in Arctic pack ice: the multiyear ice seed repository hypothesis, *J*
553 *Geophys Res-Biogeosciences*, 122(7), 1529-1548, doi: 10.1002/2016jg003668, 2017.
- 554 Peterson, A. K., Fer, I., Randelhoff, A., Meyer, A., Håvik, L., Smedsrud, L. H., Onarheim, L., Muilwijk, M., Sundfjord, A.,
555 McPhee, M. G.: N-ICE2015 Ocean turbulent fluxes from under-ice turbulence cluster (TIC) [Data set], Norwegian Polar
556 Institute, <https://doi.org/10.21334/npolar.2016.ab29f1e2>, 2016.
- 557 Reeburgh, W. S.: Fluxes Associated with Brine Motion in Growing Sea Ice, *Polar Biol.*, 3, 29-33, doi: 10.1007/Bf00265564,
558 1984.
- 559 Rinke, A., Maturilli, M., Graham, R. M., Matthes, H., Handorf, D., Cohen, L., Hudson, S. R., and Moore, J. C.: Extreme
560 cyclone events in the Arctic: Wintertime variability and trends, *Environ. Res. Letters*, 12, Artn 094006, doi:10.1088/1748-
561 9326/Aa7def, 2017.
- 562 Smith, R. E. H., Cavaletto, J. F., Eadie, B. J., and Gardner, W. S.: Growth and Lipid-Composition of High Arctic Ice Algae
563 during the Spring Bloom at Resolute, Northwest-Territories, Canada, *Mar. Ecol. Prog. Ser.*, 97, 19-29, doi:
564 10.3354/meps097019, 1993.
- 565 Takeda, S.: Influence of iron availability on nutrient consumption ratio of diatoms in oceanic waters, *Nature*, 393, 774-777,
566 doi: 10.1038/31674, 1998.
- 567 Tedesco, L., Vichi, M.: BFM-SI: a new implementation of the Biogeochemical Flux Model in sea ice. in: CMCC Research
568 Papers, <http://www.cmcc.it/publications-meetings/publications/researchpapers/rp0081-ans-03-2010>,
569 <http://hdl.handle.net/2122/5956>, 2010.
- 570 Tedesco, L., Vichi, M., and Scoccimarro, E.: Sea-ice algal phenology in a warmer Arctic, *Sci. Adv.*, 5, ARTN eaav4830, doi:
571 10.1126/sciadv.aav4830, 2019.



572 Turner, A. K., Hunke, E. C., and Bitz, C. M.: Two modes of sea-ice gravity drainage: A parameterization for large-scale
573 modeling, *J. Geophys. Res.-Oceans*, 118, 2279-2294, doi: 10.1002/jgrc.20171, 2013.

574 Urrego-Blanco, J. R., Urban, N. M., Hunke, E. C., Turner, A. K., and Jeffery, N.: Uncertainty quantification and global
575 sensitivity analysis of the Los Alamos sea ice model, *J. Geophys. Res.-Oceans*, 121, 2709-2732, doi: 10.1002/2015JC011558,
576 2016.

577 Vancoppenolle, M., C. M. Bitz, and T. Fichefet (2007), Summer landfast sea ice desalination at Point Barrow, Alaska:
578 Modeling and observations, *J. Geophys. Res.*, 112, C04022, doi:10.1029/2006JC003493.

579 Vancoppenolle, M., Bitz, C. M., and Fichefet, T.: Summer landfast sea ice desalination at Point Barrow, Alaska: Modeling
580 and observations, *J. Geophys. Res.-Oceans*, 112, Artn C04022, doi: 10.1029/2006jc003493, 2007.

581 van Leeuwe, M. A., Tedesco, L., Arrigo, K. R., Assmy, P., Campbell, K., Meiners, K. M., Rintala, J. M., Selz, V., Thomas,
582 D. N. and Stefels, J.: Microalgal community structure and primary production in Arctic and Antarctic sea ice: A synthesis.
583 *Elem. Sci. Anth.*, 6:4., doi: <https://doi.org/10.1525/elementa.267>, 2018.

584 Wakatsuchi, M., and Ono, N.: Measurements of Salinity and Volume of Brine Excluded from Growing Sea Ice, *J. Geophys.*
585 *Res.-Oceans*, 88, 2943-2951, doi: 10.1029/JC088iC05p02943, 1983.

586 Webster, M. A., Rigor, I. G., Nghiem, S. V., Kurtz, N. T., Farrell, S. L., Perovich, D. K. and Sturm, M.: Interdecadal changes
587 in snow depth on Arctic sea ice, *J. Geophys. Res.-Oceans* 119(8), 5395-5406, doi:10.1002/2014JC009985, 2014.

588

589

590

591

592

593